R. & M. No. 3717

MINISTRY OF DEFENCE (PROCUREMENT EXECUTIVE)

AERONAUTICAL RESEARCH COUNCIL
REPORTS AND MEMORANDA

An Exact Test Case for the Plane Potential Flow About Two Adjacent Lifting Aerofoils

By B. R. WILLIAMS

Aerodynamics Dept., R.A.E. Farnborough

LONDON: HER MAJESTY'S STATIONERY OFFICE

1973

PRICE £1·40 NET

An Exact Test Case for the Plane Potential Flow About Two Adjacent Lifting Aerofoils

By B. R. WILLIAMS

Aerodynamics Dept., R.A.E. Farnborough

Reports and Memoranda No. 3717*
September, 1971

Summary

A method for calculating the incompressible potential flow about two particular aerofoil sections is presented. The potential flow about two lifting circles is calculated by the method of images, and the two circles are mapped conformally on to two aerofoils by a double application of the Karman–Trefftz transformation. The results for the test cases are then compared with those from a numerical method, which uses a surface distribution of sources.

LIST OF CONTENTS

1. Introduction
2. Flow about Two Lifting Circles
   2.1. The streaming flow
   2.2. The circulating flow
   2.3. The combination flow
3. The Conformal Transformations
   3.1. Karman–Trefftz profiles
   3.2. Transformation of two circles
4. Results
   4.1. Test cases
   4.2. Comparison with A.M.O. Smith method
   4.3. Variation of the distance between the aerofoils
5. Conclusion

Symbols
References
Appendix I—Image of a doublet and a vortex in a circle
Appendix II—The geometry of two circles
Appendix III—Convergence of the series for the streaming flow
Appendix IV—Convergence of series for the circulating flow
Tables 1 to 3
Illustrations—Figs. 1 to 14
Detachable Abstract Cards

* Replaces R.A.E. Technical Report 71197—A.R.C.33 661.

1. Introduction

At present, the plane incompressible potential flow about two lifting aerofoils is calculated by numerical methods. These methods can be applied to aerofoils of arbitrary shape. However, no exact analytic solution is generally available to evaluate the accuracy of these methods. This Report presents a method of calculating an exact solution for particular configurations. The potential flow about two lifting circles is calculated, and the circles are then transformed conformally on to two aerofoils.

Previously, the potential flow about two lifting circles had been calculated by a method due to M. Lagally[1]. The region outside the two circles was transformed conformally on to a rectangular region. The complete flow was then determined by developing the image system in the sides of the rectangle. H. Strassl[2] transformed two circles on to two aerofoils, by a double application of the Karman–Trefftz transformation[3].

The method for the calculation of the flow about two circles was very complex, involving the use of elliptic functions. E. C. Maskell[4] indicated that the inherent symmetry of two circles could be used to establish a simpler solution in the plane of the two circles. This method for calculating the potential flow about two lifting circles is presented here. In fact, it was found subsequently, that W. Müller[5] had used a similar method to calculate the potential flow of a uniform stream about two nonlifting circles.

The two circles are then transformed on to two aerofoils and, by suitable choice of parameters, these may be made to resemble the wing-flap configurations used in the current work on high-lift devices[6]. Such configurations provide the desired test case, and this is illustrated by a comparison with the results of the numerical method of A. M. O. Smith[7]. The opportunity has been taken to examine the behaviour of solutions with large and small distances between the aerofoils. At either extremity, solutions for the limiting case can be obtained from single aerofoil theory, and these are used as a check on the given method.

2. Flow About Two Lifting Circles

The equations governing a potential flow are linear, thus solutions can be superposed. The flow around two lifting circles is calculated in three components: a streaming flow past both circles, a flow with a unit circulation around the first circle, and one with a unit circulation around the second circle.

2.1. The Streaming Flow

A uniform stream of unit speed is represented at the complex point z, by a complex potential, $w = z\exp(-i\alpha)$, where α is the angle of incidence of the stream to the line joining the centres of the circles (Fig. 1). The circle theorem[8] states that if a circle, $|z| = a$, is introduced into a flow, represented by the complex potential, $w = f(z)$, then the complex potential becomes

$$w = f(z) + \bar{f}\left(\frac{a^2}{z}\right). \tag{1}$$

Thus the complex potential for the flow about a circle, $|z| = a$, in a uniform stream is

$$w = z\exp(-i\alpha) + \frac{a^2\exp(i\alpha)}{z}. \tag{2}$$

The image system is a doublet of strength a^2 at A, the centre of the circle, which is the inverse of the point at infinity with respect to the first circle.

Now the second circle, $|z - f| = b$, is introduced into the flow. The circle theorem is again applied to all singularities lying outside the second circle (*see* Appendix I). The complex potential becomes

$$w = z\exp(-i\alpha) + \frac{a^2\exp(i\alpha)}{z} + \frac{b^2\exp(i\alpha)}{(z-f)} - \frac{a^2b^2\exp(-i\alpha)}{f^2(z-(f-b^2/f))}. \tag{3}$$

The additional terms can be interpreted as the image system which is formed by the reflections of the doublets outside the second circle. The reflection of the doublet at infinity is a doublet of strength b^2 at B, the centre of the second circle and the reflection of the doublet of strength a^2, at the centre of the first circle, is a doublet of strength a^2b^2/f^2 at A', the inverse point of the centre with respect to the second circle.

Now the first circle is not a streamline, thus the circle theorem is again applied to all the singularities outside the first circle, giving the complex potential

$$w = z\exp(-i\alpha) + \frac{a^2\exp(i\alpha)}{z} + \frac{b^2\exp(i\alpha)}{(z-f} - \frac{a^2b^2\exp(-i\alpha)}{f^2(z-(f-b^2/f))} - \\ - \frac{b^2a^2\exp(-i\alpha)}{f^2(z-a^2/f)} + \frac{a^2b^2a^2\exp(i\alpha)}{f^2(f-b^2/f)^2(z-(a^2/(f-b^2/f)))}. \tag{4}$$

This produces two new doublet images, which are the reflections of the images produced in the second circle by the previous step. This process is repeated and after each step either the first or the second circle is a streamline. Each reflection entails the addition of two image doublets. The set of images can be split into two groups; the first group being formed by repeated reflections of an object doublet at the centre of the first circle, and the second group originating from an object at the centre of the second circle. The strengths of the doublets in the first group are $a^2, a^2b^2/f^2, a^2b^2a^2/f^2(f-b^2/f)^2, \ldots$, whilst the second group consists of doublets strength $b^2, b^2a^2/f^2, b^2a^2b^2/f^2(f-a^2/f)^2, \ldots$.

The strength of a doublet is changed by a factor $(a/(f-t_n))^2$ for reflections in the first circle and by a factor $(b/(f-s_n))^2$ for reflections in the second circle, where s_n and t_n are the nth convergents of the continued fractions representing the distance of an object doublet from the centre of the first and second circles respectively (*see* Appendix III). Firstly, considering only reflections in the first circle, the object doublet lies inside the second circle, thus

$$t_n < b,$$

therefore

$$\frac{a}{(f-t_n)} < \frac{a}{f-b}. \tag{5}$$

The circles do not overlap, thus

$$f - b > a,$$

therefore

$$\frac{a}{f-b} < 1. \tag{6}$$

Similarly it can be shown that

$$\frac{b}{f-s_n} < \frac{b}{f-a} < 1.$$

After $2n$ reflections, the strength of a doublet from the first group is less than $a^2\{a^2/(f-b)^2\}^n \times \{b^2/(f-a)^2\}^n$.

Now

$$\lim_{n\to\infty} a^2 \left\{\frac{a^2}{(f-b)^2}\right\}^n \left\{\frac{b^2}{(f-a)^2}\right\}^n = 0. \tag{7}$$

The strength of the doublets, which are added after each reflection, is monotonic decreasing and approaches zero. After several reflections, the new image doublets will only slightly change the complex potential of the system. This establishes a necessary condition for the series to converge to the complex potential for the streaming flow past two circles. The proof of a sufficient condition for convergence is given in Appendix III.

2.2. The Circulating Flow

A flow with unit circulation around the first circle is constructed by placing a unit vortex at A, the centre of the first circle (Fig. 2). The second circle is now introduced into the flow and is made into a streamline by use of the circle theorem (*see* Appendix I) which gives the complex potential

$$w = i \log z + i \log (z - f) - i \log \left(z - \left(f - \frac{b^2}{f} \right) \right), \tag{8}$$

where $(f - b^2/f)$, A', is the inverse of the centre of the first circle with respect to the second circle. The image system consists of a vortex, strength -1, at the inverse point and a vortex, strength $+1$, at the centre. Thus there is no circulation around the second circle.

Now the first circle is not a streamline and the circle theorem is again applied to all the singularities outside the first circle, giving the complex potential

$$w = i \log z + i \log (z - f) - i \log \left(z - \left(f - \frac{b^2}{f} \right) \right) - i \log \left(z - \frac{a^2}{f} \right) + i \log \left(z - \frac{a^2}{f - b^2/f} \right), \tag{9}$$

where a^2/f, B', is the inverse of the centre of the second circle with respect to the first circle and $a^2/(f - b^2/f)$ is the inverse of $(f - b^2/f)$ with respect to the first circle. The image system consists of a vortex, strength $+1$, at $a^2/(f - b^2/f)$; a vortex, strength -1, at a^2/f and two vortices of opposite strength at the centre, which cancel each other out.

This process is repeated, alternatively making the first and second circles streamlines. Unfortunately the strength of the vortices does not diminish after each reflection. However, each reflection effectively entails the addition of two vortices of opposite sense at inverse points in one of the circles. In Appendix II, it is shown that the set of inverse points in a circle converges on to the complementary inverse point. Thus the image system which is added after each reflection, approaches a vortex doublet, for which the complex potential is zero. This constitutes a necessary condition for the complex potential of the above system to converge to the complex potential for a flow with unit circulation around the first circle. A proof of sufficiency is given in Appendix IV. A similar method is used to determine the complex potential for a flow with unit circulation around the second circle. The series for the streaming and circulating flows converge rapidly, and in all the calculations the series are truncated, when the variation in the complex potential, due to the addition of the next term, is less than 10^{-8}. The resulting values represent a good numerical approximation to the exact value of the complex potential. The numerical approximation can be made as close to the exact value, as is desired, by increasing the number of terms in the truncated part of the series.

2.3. The Combination Flow

The complete flow around the two circles is a linear combination of the three component solutions. The coefficients of the linear combination, the circulations, are determined by considering the velocities at the points T_1 and T_2, where T_1 and T_2 are the points on the two circles which transform on to the trailing edges of the two aerofoils. The velocities at these points are given by

$$V(T_1) = V_0(T_1) + \Gamma_1 V_{\Gamma_1}(T_1) + \Gamma_2 V_{\Gamma_2}(T_1) \tag{10}$$

and

$$V(T_2) = V_0(T_2) + \Gamma_1 V_{\Gamma_1}(T_2) + \Gamma_2 V_{\Gamma_2}(T_2), \tag{11}$$

where V_0 is the velocity due to the stream flow,
V_{Γ_1} is the velocity due to a unit circulation around the first circle,
V_{Γ_2} is the velocity due to a unit circulation around the second circle,
Γ_1 is the circulation around the first circle and
Γ_2 is the circulation around the second circle.

To avoid infinite velocities in the final solution, the points T_1 and T_2 must be stagnation points. Thus the circulations are given by,

$$\Gamma_1 = \frac{V_{\Gamma_2}(T_1)V_0(T_2) - V_{\Gamma_2}(T_2)V_0(T_1)}{V_{\Gamma_1}(T_1)V_{\Gamma_2}(T_2) - V_{\Gamma_1}(T_2)V_{\Gamma_2}(T_1)} \tag{12}$$

and

$$\Gamma_2 = \frac{V_{\Gamma_1}(T_1)V_0(T_2) - V_{\Gamma_1}(T_2)V_0(T_1)}{V_{\Gamma_2}(T_2)V_{\Gamma_2}(T_1) - V_{\Gamma_1}(T_1)V_{\Gamma_2}(T_2)}. \tag{13}$$

In the calculation of the component flows, the line joining the centres of the two circles is an axis of symmetry. The calculations are performed relative to this line. The flow about the two circles, relative to the coordinate system which is used for the conformal mappings, is calculated by the introduction of a virtual angle of incidence, δ (*see* Section 3.2).

3. The Conformal Transformations

3.1. Karman–Trefftz Profiles

The conformal transformation

$$\frac{\zeta - nc}{\zeta + nc} = \left\{\frac{z - c}{z + c}\right\}^n, \tag{14}$$

maps a circle in the z-plane on to a Karman–Trefftz profile[3] in the ζ-plane (Fig. 3). The critical points $M(-c, 0)$ and $N(c, 0)$ transform on to $M'(-nc, 0)$ and $N'(nc, 0)$ respectively. The point P, which subtends an angle ϕ to the line MN, transforms on to the point P', which subtends an angle $n\phi$ to the line $M'N'$. The centre of the circle is

$$x = a \sin \beta, \qquad y = a \cos \beta - c,$$

where a is the radius of the circle,
c is the arbitrary length defining scale and
β is the angle between the radius, ON, and the x-axis.

The camber of the aerofoil is determined by the angle, β, and the thickness by the ratio, a/c. The trailing-edge angle, τ, is $(2 - n)\pi$ radians. Thus the Karman–Trefftz profile is completely defined by the parameters β, $k(= a/c)$, n.

3.2. Transformation of Two Circles

Two circles in the z-plane are transformed conformally on to two aerofoils in the ζ-plane in the following manner. The first circle, radius a, has its centre at the point $(c_1 - a \cos \beta_1, a \sin \beta_1)$, whilst the

second circle, radius b, has its centre at the point

$$(x_2, y_2) = (f\cos\delta + c_1 - a\cos\beta_1, f\sin\delta - a\sin\beta_1)$$

where δ is the angle of declination of the centre of the second circle to the centre of the first circle (*see* Fig. 4).

The first circle is transformed on to a Karman–Trefftz profile for which the parameters of transformation are β_1, k_1 and n_1. The shape of the second circle is almost unchanged, since the Jacobian and the area magnification factor of the transformation are nearly constant in this region.

The angle of flap deflection in the final configuration is required to be $\bar{\eta}$, thus the profiles are rotated about the centre of the second circle, through an angle $\bar{\eta}$, before the second circle is transformed on to a Karman–Trefftz profile, with transformation parameters β_2, k_2 and n_2. The two aerofoils are then transformed so that the leading edge of the first aerofoil is at the origin and the chord of the first aerofoil, which is scaled to unity, lies along the ξ-axis.

The coordinates of the points T_1 and T_2, which transform on to the trailing edge of the main aerofoil and flap respectively, are given below

	T_1	T_2
x	c_1	$x_2 + b\cos(-\beta_2 - \bar{\eta})$
y	0	$y_2 + b\sin(-\beta_2 - \bar{\eta})$

If q_z is the speed at a point in the z-plane, then the speed, q_ζ, at the corresponding point in the plane of the two aerofoils is given by

$$q_\zeta = \frac{q_z}{|dm/dz|\,|d\zeta/dm|} \tag{15}$$

where m is the complex variable in the intermediate plane,
$|dm/dz|$ is the Jacobian of the first transformation and
$|d\zeta/dm|$ is the Jacobian of the second transformation.

The pressure coefficient, C_p, at the point is then calculated by the relationship,

$$C_p = 1 - q_\zeta^2. \tag{16}$$

The forces normal and parallel to the axis, C_N and C_A respectively, are calculated by integrating a linear approximation of the pressure distribution.

4. Results

In all the following cases, the parameters of the two Karman–Trefftz transformations were kept constant, since these parameters produced the required shapes. A different choice could have been used to generate different shapes. The parameters for the transformation are given in Table 1(a). The first circle was placed at the origin and had a radius of 1·096. The definition of the configuration was then completed by the specification of the position and radius of the second circle and the flap deflection.

4.1. Test Cases

The flow around two circles, for which the geometry is specified in Table 1(b), was calculated. The position of the stagnation points fixed the circulation around the two circles and the values are given in Table 1(c). The pressure distributions for a flow at zero angle of incidence are shown in Figs. 5 and 6.

Figure 7 shows the streamlines about the two circles, which were determined by extensive calculation of the stream function. Figure 8 gives configuration A, which results from a transformation of these circles, associated with a flap deflection of 30 degrees. The pressure distributions about the main wing and flap are given in Figs. 9 and 10. The coordinates and pressure coefficients are also given in Table 2(a).

To derive a configuration with a flap deflection of 10 degrees, two new stagnation points were specified (*see* Table 1(d)). This produced the configuration B, of Fig. 8. The pressure distributions about this configuration are given in Figs. 11 and 12. The coordinates and pressure distributions are again given in Table 2(b).

The forces and circulations for the two configurations are given below. The total drag is zero, which is consistent with the assumption of potential flow.

	Main aerofoil			Flap		
	C_L	C_D	Γ	C_L	C_D	Γ
Configuration A 30° flap	2·9065	−0·3839	1·3909	0·8302	0·3838	0·4784
Configuration B 10° flap	1·6915	−0·0898	0·8400	0·3366	0·0897	0·1745

4.2. Comparison with A. M. O. Smith Method

By way of an illustration of the use of these test cases, the flows around configurations A and B have been calculated by the numerical method of A. M. O. Smith with 121 points on the main aerofoil and 61 points on the flap. The points were selected, at regular spacing around the aerofoil, by a cubic spline interpolation[9]. Comparisons of the pressure distributions are given in Figs. 9, 10, 11 and 12, whilst the forces and circulations are compared in Table 3. The comparisons for flap angles of 20 degrees and 40 degrees are also given. The pressure distributions around two circles are compared with the test cases in Figs. 5 and 6.

The agreement with the exact solution is very good for the two circles; whereas the discontinuities in slope and curvature at the trailing edges of both aerofoils cause small errors in the A. M. O. Smith method. However, the errors are small enough for the A. M. O. Smith method to be used for the calculation of potential flow about two aerofoils.

4.3. Variation of the Distance Between the Aerofoils

The nature of the solution at very large and very small separations was studied. In both situations, the solutions for the limiting cases could be obtained from single aerofoil theory. The separation between the aerofoils was measured by the parameter d, the minimum distance between the perimeters of the circles.

The distance between the aerofoils was increased and the flow at 10 degrees incidence calculated. In Fig. 13, the lift is plotted against the inverse of the parameter, d. It can be seen that the force on the wing increases as the separation between the two aerofoils is decreased, whilst the force on the flap decreases with the separation. The reduction in the force on the flap implies a reduction in adverse pressure gradient on the flap. This will provide some compensation for the increased interference between the viscous wake of the wing and the viscous layer on the flap, which was noted in some recent experiments[6]. The flow about the single aerofoils was calculated by the Karman–Trefftz method[3]. In both cases this provided the limiting value of the lifts obtained by the two aerofoil solution. At large separations one aerofoil does not influence the flow around the second aerofoil, thus the result is trivial. However it provided a useful means of checking the computer program developed for the method.

The distance between the aerofoils was reduced and the flow at 0 degrees incidence calculated. In Fig. 14a it can be seen that the stream functions on both aerofoils approached the same limiting value smoothly. The total lift on the two aerofoils also attained a maximum value before they touched (Fig. 14b). The aerofoil shapes corresponding to $d = 0{\cdot}038$ were faired together, producing a single stream surface. The exact flow about this single aerofoil was calculated by the method due to Catherall, Foster and Sells[10]. The fairing was not expected to change the flow field greatly, since Fig. 14a indicated that the streamline pattern would not be appreciably changed. The change in the flow field was reflected in a small difference in total C_L, but this comparison was still considered to be a useful check on the computer program.

5. Conclusion

The transformation of two circles, by a double application of the Karman–Trefftz transformation, produced satisfactory profiles. The flow about the two circles could be expressed analytically in the form of an infinite series, which converged rapidly. A numerical approximation to any required degree of accuracy was obtained by considering a sufficiently large number of terms from the series. The flow about two particular configurations was calculated and these could be used as test cases for numerical methods. The solution by the A. M. O. Smith method was compared with the exact solutions. The agreement was good, confirming that the numerical method of A. M. O. Smith can be used for the calculation of potential flow about two arbitrary aerofoils.

LIST OF SYMBOLS

A	Centre of first circle
A'	Inverse of A with respect to the second circle
a	Radius of first circle
B	Centre of second circle
B'	Inverse of B with respect to the first circle
b	Radius of first circle
c	Arbitrary length defining scale
C_A	Integrated force parallel to axis
C_D	Integrated force parallel to direction of stream
C_L	Integrated force normal to direction of stream
C_N	Integrated force normal to axis
C_p	Pressure coefficient
d	Minimum distance between circles
f	Distance between the centres of the two circles
k	a/c
M	Critical point of Karman–Trefftz transformation
M'	Transformed critical point, M
m	Complex variable of intermediate transformation plane
N	Critical point of Karman–Trefftz transformation
N'	Transformed critical point, N
n	$2 - \tau/\pi$
P	Point on circle
P'	Point on Karman–Trefftz profile
p	Arbitrary positive integer
q	Point outside circle
q_ζ	Speed at a point in the ζ-plane
q_z	Speed at a point in the z-plane
r	Radius of circle
S	Complementary inverse point of first circle
s	Distance of S from centre of first circle
$\{s_n\}$	Sequence of inverse points in first circle
s_∞	Limit of sequence $\{s_n\}$
T	Complementary inverse point of second circle
t	Distance of T from centre of second circle

$\{t_n\}$	Sequence of inverse points in second circle
t_∞	Limit of sequence $\{t_n\}$
$T_i (i = 1, 2)$	Point on circle which transforms onto the trailing edge
u_n	nth term in a series
V_p	pth partial sum of a series
V	Combination velocity
V_0	Velocity due to stream flow
V_{Γ_1}	Velocity due to a flow with unit circulation around the first circle
V_{Γ_2}	Velocity due to a flow with unit circulation around the second circle
w	Complex potential
X_1	Point inside first circle
X_1'	Inverse of X_1 with respect to the second circle
x_1	Distance of X_1 from centre of first circle
x, y	Cartesian coordinates in the plane of the two circles
x_2, y_2	Centre of second circle
z	$x + iy$
α	Angle of incidence
β	Angle determining camber of Karman–Trefftz profile
δ	Declination of centre of second circle with respect to the centre of the first circle
ε	Arbitrarily small positive number
$\Gamma_i (i = 1, 2)$	Circulation around circle
$\bar{\eta}$	Angle of deflection of the flap
ζ	$\xi + i\eta$, complex variable in physical plane
τ	Trailing-edge angle
ϕ	Angle subtended at point P by line MN

REFERENCES

No.	Author(s)	Title, etc.
1	M. Lagally	Die eibungslose Strömung im Aussengebiete zweier Kreise. Z.A.M.M. Vol. 9 (1929). (Translated in N.A.C.A. T.M. 626.)
2	H. Strassl	Die ebene Potentialströmung um ein Flügelprofil mit Vorflügel. Jahrbuch 1939 der deutschen Luftfahrtforschung.
3	H. Glauert	A generalised type of Joukowski aerofoil. A.R.C. R. & M. No. 911 (1924).
4	E. C. Maskell	Private communication.
5	W. Müller	Systeme von Doppelquellen in der ebenen strömung, insbesondere die strömung um zwei Kreizylinder. Z.A.M.M. Vol. 9 (1929).
6	D. N. Foster, ... H. P. A. H. Irwin and B. R. Williams	The twodimensional flow around a slotted flap. A.R.C. R. & M. No. 3681 (1970).
7	J. L. Hess and .. .. A. M. O. Smith	Calculation of potential flow about arbitrary bodies. *Progress in Aeronautical Sciences* Vol. 8, Pergamon Press, London (1966).
8	L. M. Milne-Thomson ..	Theoretical hydrodynamics. Macmillan & Co. Ltd. (1955).
9	J. M. Freeland	Cubic spline fitting. R.A.E. Math Computing Notes, Series C335 (1965).
10	D. Catherall, D. N. Foster and C. C. L. Sells	Twodimensional incompressible flow past a lifting aerofoil. R.A.E. Technical Report 69118, A.R.C. 31545 (1969).
11	G. H. Hardy	A course of pure mathematics. Cambridge University Press (1948).

APPENDIX I

Image of a Doublet and a Vortex in a Circle

The circle theorem is used to obtain the image systems of a doublet and a vortex in a circle. The circle may, without loss of generality, be taken to have its centre at the origin and radius r.

Image of a Doublet

The complex potential of a doublet of unit strength and inclination, α, at a point q, outside the circle is

$$w = \frac{\exp(i\alpha)}{z - q}. \tag{I.1}$$

On introduction of the circle, $|z| = r$, the complex potential becomes

$$w = \frac{\exp(i\alpha)}{(z - q)} + \frac{\exp(-i\alpha)}{r^2/z - q}. \tag{I.2}$$

The complex potential is only defined to within a constant, thus it may be written

$$\begin{aligned} w &= \frac{\exp(i\alpha)}{(z - q)} + \frac{\exp(-i\alpha)}{(r^2/z - q)} + \frac{1}{q}\exp(-i\alpha) \\ &= \frac{\exp(i\alpha)}{(z - q)} + \exp(-i\alpha)\left\{\frac{1}{(r^2/z - q)} + \frac{z}{qz}\right\} \\ &= \frac{\exp(i\alpha)}{(z - q)} + \exp(-i\alpha)\left\{\frac{r^2}{(r^2 - qz)q}\right\}. \end{aligned}$$

The inverse point, q', is defined such that $r^2 = qq'$.

$$w = \frac{\exp(i\alpha)}{(z - q)} - \frac{r^2}{q^2}\frac{\exp(-i\alpha)}{(z - q')}. \tag{I.3}$$

The image is a doublet of strength r^2/q^2 and inclination, $-\alpha$, at the inverse point.

Image of a Vortex

The complex potential of a unit vortex at a point, q, outside the circle, is

$$w = i\log(z - q).$$

On introduction of the circle, $|z| = r$, the complex potential becomes

$$\begin{aligned} w &= i\log(z - q) - i\log\left(\frac{r^2}{z} - q\right) \\ &= i\log(z - q) + i\log\left(\frac{z}{r^2 - zq}\right) \\ &= i\log(z - q) + i\log(z) - i\log\left(z - \frac{r^2}{q}\right) + \text{const.} \end{aligned} \tag{I.5}$$

The image system is a vortex of opposite sense at the inverse point and a vortex of the same sense at the centre.

APPENDIX II

The Geometry of Two Circles

Consider two circles with their centres at A, the origin, and $B(f, 0)$. Let their radii be a and b respectively (*see* Fig. 1). Two points are defined as inverse points with respect to a circle, if the product of their distances from the centre is the square of the radius. Thus the points X_1 and X'_1 are inverse points with respect to the second circle, because their distances from the centre are $f - x_1$ and $b^2/(f - x_1)$ respectively.

The points S and T are called complementary inverse points, if S is the inverse of T with respect to the first circle and T is the inverse of S with respect to the second circle. For this situation

$$\frac{a^2}{f - b^2/(f - s)} = s \tag{II.1}$$

where s is the distance of S from the centre of first circle. Hence

$$fs^2 - (a^2 - b^2 - f^2)s + a^2 f = 0$$

and

$$s = \frac{(a^2 - b^2 + f^2) \pm \sqrt{(a^2 - b^2 + f^2)^2 - 4a^2 f^2}}{2f}.$$

The roots define the distances of S and T from the centre of the first circle.

Consider the set of inverse points inside the first circle, which are defined by the repeated reflections of the centres of the two circles (*see* Section 2.1). Let this sequence be $\{s_n\}$, where

$$s_1 = \frac{a^2}{f}, \qquad s_2 = \frac{a^2}{f - b^2/f}, \qquad s_3 = \frac{a^2}{f - (b^2/(f - a^2/f))} \cdots\cdots \tag{II.3}$$

The terms s_{2n} are reflections of an object at the centre of the first circle and the terms s_{2n+1} originate from the centre of the second circle.

All the inverse points lie inside the first circle, therefore

$$s_n < a. \tag{II.4}$$

Now

$$f - \frac{b^2}{f} < f$$

therefore

$$\frac{a^2}{f} < \frac{a^2}{f - b^2/f}$$

i.e.

$$s_1 < s_2.$$

Similarly

$$s_2 < s_3$$

and, in general,

$$s_n < s_{n+1}. \tag{II.5}$$

The sequence is monotonic increasing and bounded above, thus it converges to a limit, s_∞. The infinite continued fraction may be written in the following form

$$s_\infty = \frac{a^2}{f - b^2/(f - s_\infty)}, \tag{II.6}$$

hence

$$fs_\infty^2 - (a^2 - b^2 + f^2)s_\infty + a^2 f = 0$$

and

$$s_\infty = \frac{(a^2 - b^2 + f^2) \pm \sqrt{(a^2 - b^2 + f^2)^2 - 4a^2f^2}}{2f}.$$

By comparison with equation (II.2), it can be seen that the sequence of inverse points in each circle will converge to a limit, which is the complementary inverse point for that circle.

APPENDIX III

Convergence of the Series for the Streaming Flow

The series for the complex potential of the streaming flow is

$$w = z\exp(-i\alpha) + \frac{a^2\exp(i\alpha)}{z} + \frac{b^2\exp(i\alpha)}{(z-f)} - \frac{a^2b^2\exp(-i\alpha)}{f^2[z-(f-b^2/f)]} -$$

$$\frac{b^2a^2\exp(-i\alpha)}{f^2\left(z-\frac{a^2}{f}\right)} + \frac{a^2b^2a^2\exp(i\alpha)}{f^2\left(f-\frac{b^2}{f}\right)^2\left(z-\frac{a^2}{f-b^2/f}\right)} + \frac{b^2a^2b^2\exp(i\alpha)}{f^2\left(f-\frac{a^2}{f}\right)^2\left(z-\left(f-\frac{b^2}{f-a^2/f}\right)\right)} -$$

$$\frac{a^2b^2a^2b^2\exp(-i\alpha)}{f^2\left(f-\frac{b^2}{f}\right)^2\left(f-\frac{a^2}{f-b^2/f}\right)^2\left(z-\left(f-\frac{b^2}{f-[a^2/(f-b^2/f)]}\right)\right)} + \ldots. \tag{III.1}$$

Let

$$s_1 = \frac{a^2}{f}, \qquad s_2 = \frac{a^2}{f-b^2/f}, \qquad s_3 = \frac{a^2}{f-[b^2/(f-a^2/f)]}, \ldots \tag{III.2}$$

and

$$t_1 = \frac{b^2}{f}, \qquad t_2 = \frac{b^2}{f-a^2/f}, \qquad t_3 = \frac{b^2}{f-[a^2/(f-b^2/f)]}, \tag{III.3}$$

where s_n represents an inverse point inside the first circle and t_n represents an inverse point inside the second circle. In Appendix II, it was proved that the sequences $\{s_n\}$ and $\{t_n\}$ tend to the limits s and t, the complementary inverse points.

The series may be rewritten as

$$|w| \leqslant |z| + \frac{a^2}{|z|} + \frac{b^2}{|z-f|} + \frac{a^2b^2}{f^2|(z-(f-t_1))|} + \frac{b^2a^2}{f^2|(z-s_1)|} + \frac{a^2b^2a^2}{f^2(f-t_1)^2|(z-s_2)|} +$$

$$+\frac{b^2a^2b^2}{f^2(f-s_1)^2|(z-(f-t_2))|} + \frac{a^2b^2a^2b^2}{f^2(f-t_1)^2(f-s_2)^2}\frac{1}{|(z-(f-t_3))|} + \ldots. \tag{III.4}$$

Now

$$\frac{|a|}{|f-t_n|} < \frac{|a|}{|f-b|} < 1 \qquad (\textit{see} \text{ Section 2.1}).$$

Similarly

$$\frac{|b|}{|f-s_n|} < \frac{|b|}{|f-a|} < 1$$

therefore

$$|w| \leqslant |z| + \frac{a^2}{|z|} + \frac{b^2}{|z|} + \frac{a^2b^2}{f^2|z|} + \frac{b^2a^2}{f^2|z|} + \frac{a^2b^2a^2}{f^2(f-b)^2}\frac{1}{|z|} + \frac{b^2a^2b^2}{f^2(f-a)^2}\frac{1}{|z|} +$$

$$+ \frac{a^2b^2a^2b^2}{f^2(f-b)^2(f-a)^2}\frac{1}{|z|} + \ldots . \qquad \text{(III.5)}$$

Now Dirichlet's theorem states that the sum of a series of positive terms is the same in whatever order the terms are taken, thus rearranging

$$|w| \leqslant |z| + \frac{a^2}{|z|} + \frac{a^2b^2}{f^2|z|} + \frac{a^2b^2a^2}{f^2(f-b)^2}\frac{1}{|z|} + \frac{a^2b^2a^2b^2}{f^2(f-b)^2(f-a)^2}\frac{1}{|z|} + \ldots$$

$$+ \frac{b^2}{|z|} + \frac{b^2a^2}{f^2|z|} + \frac{b^2a^2b^2}{f^2(f-a)^2}\frac{1}{|z|} + \ldots . \qquad \text{(III.6)}$$

This series is convergent by the ratio test. Thus, by comparison, the series for the complex potential of the stream flow is absolutely convergent.

APPENDIX IV

Convergence of Series for the Circulating Flow

The series for the complex potential of a flow with unit circulation around the first circle is

$$w = i\log z + i\log(z-f) - i\log\left\{z-\left(f-\frac{b^2}{f}\right)\right\} + i\log\left\{z-\left(\frac{a^2}{f-b^2/f}\right)\right\} - i\log\left\{z-\frac{a^2}{f}\right\} + \ldots . \tag{IV.1}$$

This series may be rewritten as

$$w = i\log z + i\log(z-f) - i\log(z-(f-t_1)) + i\log(z-s_2) - i\log(z-s_1) + \ldots$$

where

$$\lim_{n\to\infty}(f-t_n) = f-t$$

and

$$\lim_{n\to\infty} s_n = s \text{ (}see\text{ Appendix III).}$$

In general, the modulus of terms in this series do not approach zero. Thus the series is not absolutely convergent (Abel's theorem[11]). The series is either conditionally convergent or absolutely divergent. A conditionally convergent series can always be so rearranged as to converge to any sum whatever, or to diverge. By reference to the physical definition of this series, the terms must be grouped in the following fashion

$$w = i\log z + \{i\log(z-f) - i\log(z-(f-t_1))\} + \{i\log(z-s_2) - i\log(z-s_1)\} + \ldots , \tag{IV.3}$$

where each grouping represents the addition of one set of images. This series may be expressed more concisely as

$$w = i\log z + i\log\left\{\frac{z-f}{z-(f-t_1)}\right\} + \sum_{n=1}^{\infty}\left[i\log\left\{\frac{z-s_{2n}}{z-s_{2n-1}}\right\} + i\log\left\{\frac{z-(f-t_{2n})}{z-(f-t_{2n+1})}\right\}\right]. \tag{IV.5}$$

Now

$$\lim_{n\to\infty}\left\{\frac{z-s_{2n}}{z-s_{2n-1}}\right\} = 1 \tag{IV.5}$$

and

$$\lim_{n\to\infty}\left\{\frac{z-(f-t_{2n})}{z-(f-t_{2n+1})}\right\} = 1. \tag{IV.6}$$

In general, the modulus of the terms in this series approaches zero. This is a necessary condition for convergence.

The series may be rewritten as

$$w = i\log z + i\log\left\{\frac{z-f}{z-(f-t_1)}\right\} + \sum_{n=1}^{\infty} i\log\left\{1+\frac{s_{2n-1}-s_{2n}}{z-s_{2n-1}}\right\} +$$

$$+ \sum_{n=1}^{\infty} i\log\left\{1+\frac{t_{2n}-t_{2n+1}}{z-(f-t_{2n+1})}\right\}. \tag{IV.7}$$

It can be shown that the series $\sum_{n=0}^{\infty}\log(1+u_n)$ converges absolutely if, and only if, the series $\sum|u_n|$ is convergent[11].

Let

$$\frac{s_{2n-1}-s_{2n}}{z-s_{2n-1}} = u_n \tag{IV.8}$$

and

$$v_p = \sum_{n=1}^{p} u_n. \tag{IV.9}$$

Now for the region outside the first circle

$$|z-s_n| > |a-s|,$$

therefore

$$\left|\frac{s_{2n-1}-s_{2n}}{z-s_{2n-1}}\right| < \frac{|s_{2n-1}-s_{2n}|}{|a-s|}. \tag{IV.10}$$

There exists a positive integer N, such that for all values of $n \geqslant N$ and for all positive integer values of p

$$|V_{p+n}-V_n| \leqslant \left|\frac{s_{2(n+p)-1}-s_{2(n+p)}}{a-s}\right| + \left|\frac{s_{2(n+p-1)-1}-s_{2(n+p-1)}}{a-s}\right| + \ldots + \left|\frac{s_{2n-1}-s_{2n}}{a-s}\right|. \tag{IV.11}$$

Now $\{s_n\}$ is convergent, thus for all $[(a-s)\varepsilon/p] > 0$, where ε is an arbitrarily small positive number, and for all $n \geqslant N$

$$|s_{n+1}-s_n| < \frac{(a-s)\varepsilon}{p}. \tag{IV.12}$$

Thus equation (IV.11) becomes

$$|V_{p+n}-V_n| < p\frac{(a-s)\varepsilon}{p}\frac{1}{(a-s)} = \varepsilon. \tag{IV.13}$$

The sequence of partial sums of the series $\sum|u_n|$ is convergent, therefore the series $\sum|u_n|$ is convergent. Similarly it can be proved that

$$\sum_{n=1}^{\infty} i\log\left\{1+\frac{t_{2n}-t_{2n+1}}{z-(f-t_{2n+1})}\right\}$$

is convergent and it follows that the series (IV.7) is convergent. In summary, the rearrangement of the series for the circulating flow, which is suggested by the physical definition of the problem, is absolutely convergent.

TABLE 1

(a) Parameters for transformations

	β	k	τ
First transformation	0·001	1·096	0·17279
Second transformation	0·08725	1·15	0·17279

(b) Geometry of circles

		First circle	Second circle
Centre	X	0·0	1·9
	Y	0·0	−0·4
Radius		1·096	0·5

(c) Configuration A: 30° flap

Stagnation points	X	1·0727	2·4015
	Y	0·2247	−0·1963
Circulation		5·169	1·778

(d) Configuration B: 10° flap

Stagnation points	X	1·0727	2·4409
	Y	0·2247	−0·0271
Circulation		3·154	0·655

TABLE 2(a)

Configuration A: Main Aerofoil

ξ	η	C_p
0·99931	0·00612	−0·04022
0·99417	0·00748	0·23687
0·98434	0·00903	0·50061
0·96975	0·00941	0·67369
0·94998	0·00766	0·75477
0·92461	0·00361	0·77689
0·89358	−0·00236	0·76914
0·85728	−0·00965	0·74766
0·81639	−0·01771	0·72058
0·77169	−0·02612	0·69205
0·72396	−0·03451	0·66437
0·67396	−0·04261	0·63898
0·62240	−0·05018	0·61699
0·56993	−0·05699	0·59936
0·51716	−0·06287	0·58708
0·46466	−0·06766	0·58115
0·41297	−0·07214	0·58264
0·36259	−0·07350	0·59271
0·31398	−0·07438	0·61252
0·26759	−0·07386	0·64327
0·22381	−0·07194	0·68596
0·18304	−0·06866	0·74118
0·14563	−0·06409	0·80830
0·11190	−0·05833	0·88385
0·08214	−0·05151	0·95724
0·05663	−0·04378	0·99969
0·03560	−0·03530	0·93296
0·01927	−0·02625	0·53705
0·00783	−0·01681	−0·79779
0·00143	−0·00714	−4·20249
0·00017	0·00264	−8·34989
0·00409	0·01242	−8·73166
0·01311	0·02211	−7·14534
0·02707	0·03155	−5·73037
0·04582	0·04056	−4·73940
0·06914	0·04898	−4.05084
0·09681	0·05663	−3·55471
0·12857	0·06335	−3·18166
0·16414	0·06902	−2·88974
0·20321	0·07352	−2·65315
0·24543	0·07678	−2·45564
0·29044	0·07875	−2·28674
0·33785	0·07942	−2·13965
0·38724	0·07881	−2·00992
0·43814	0·07700	−1·89477
0·49010	0·07408	−1·79260
0·54258	0·07019	−1·70272
0·59507	0·06550	−1·62525
0·64697	0·06020	−1·56109
0·69769	0·05453	−1·51204
0·74656	0·04870	−1·48106
0·79290	0·04293	−1·47265
0·83597	0·03743	−1·49342
0·87501	0·03232	−1·55225
0·90929	0·02762	−1·65810
0·93815	0·02323	−1·80900
0·96122	0·01893	−1·95727
0·97850	0·01458	−1·95374
0·99043	0·01041	−1·60169
0·99753	0·00718	−0·02119
1·00000	0·00590	1·0000

TABLE 2(a) (Contd.)

Configuration A: Flap

ξ	η	C_p
1·31360	−0·20335	0·61683
1·31121	−0·20083	0·62318
1·30635	−0·19598	0·64997
1·29886	−0·18893	0·67827
1·28864	−0·17996	0·70420
1·27564	−0·16939	0·72668
1·25995	−0·15765	0·74560
1·24177	−0·14518	0·76122
1·22146	−0·13243	0·77401
1·19948	−0·11982	0·78457
1·17640	−0·10766	0·79358
1·15285	−0·09619	0·80184
1·12944	−0·08553	0·81022
1·10676	−0·07572	0·81976
1·08535	−0·06674	0·83159
1·06565	−0·05854	0·84699
1·04799	−0·05105	0·86722
1·03263	−0·04423	0·89341
1·01972	−0·03807	0·92597
1·00930	−0·03258	0·96308
1·00134	−0·02781	0·99520
0·99572	−0·02381	0·98154
0·99226	−0·02065	0·71658
0·99073	−0·01835	−1·17476
0·99087	−0·01686	−5·75997
0·99242	−0·01604	−2·85918
0·99508	−0·01571	−1·43049
0·99864	−0·01569	−0·89891
1·00295	−0·01582	−0·70367
1·00797	−0·01598	−0·68332
1·01372	−0·01607	−0·77990
1·02027	−0·01609	−0·96299
1·02768	−0·01606	−1·20757
1·03600	−0·01610	−1·48844
1·04527	−0·01631	−1·78052
1·05548	−0·01684	−2·06103
1·06658	−0·01785	−2·31124
1·07852	−0·01946	−2·51744
1·09119	−0·02181	−2·67093
1·10447	−0·02499	−2·76751
1·11824	−0·02909	−2·80664
1·13235	−0·03415	−2·79067
1·14667	−0·04020	−2·72396
1·16103	−0·04725	−2·61232
1·17532	−0·05525	−2·46235
1·18938	−0·06416	−2·28112
1·20310	−0·07391	−2·07571
1·21637	−0·08439	−1·85307
1·22907	−0·09548	−1·61970
1·24112	−0·10704	−1·38159
1·25245	−0·11891	−1·14405
1·26298	−0·13090	−0·91168
1·27267	−0·14281	−0·68829
1·28147	−0·15440	−0·47687
1·28934	−0·16544	−0·27961
1·29624	−0·17566	−0·09789
1·30214	−0·18476	0·06777
1·30697	−0·19245	0·21788
1·31064	−0·19840	0·35456
1·31303	−0·20226	0·48483
1·31389	−0·20363	1·0000

TABLE 2(b)

Configuration B: Main Aerofoil

ξ	η	C_p	ξ	η	C_p
0·99909	−0·02602	0·58198	0·00409	0·01226	−3·28388
0·99238	−0·02395	0·67724	0·01303	0·02179	−3·13648
0·97992	−0·02084	0·75444	0·02687	0·03106	−2·77164
0·96239	−0·01796	0·78703	0·04543	0·03989	−2·45446
0·94007	−0·01646	0·77650	0·06852	0·04811	−2·20772
0·91295	−0·01692	0·73463	0·09589	0·05554	−2·01489
0·88103	−0·01938	0·67631	0·11111	0·05892	−1·93332
0·84454	−0·02353	0·61326	0·14445	0·06489	−1·79172
0·80395	−0·02892	0·55202	0·18139	0·06972	−1·67118
0·75984	−0·03509	0·49525	0·22162	0·07332	−1·56525
0·71287	−0·04167	0·44372	0·26478	0·07563	−1·46976
0·66372	−0·04828	0·39755	0·31051	0·07660	−1·38202
0·61304	−0·05463	0·35678	0·35839	0·07623	−1·30038
0·56146	−0·06045	0·32161	0·40798	0·07457	−1·22392
0·50955	−0·06551	0·29245	0·45884	0·07168	−1·15226
0·45790	−0·06936	0·26996	0·51048	0·06765	−1·08542
0·40701	−0·07266	0·25500	0·56237	0·06263	−1·02376
0·35739	−0·07447	0·24869	0·61396	0·05676	−0·96791
0·30950	−0·07499	0·25236	0·66469	0·05023	−0·91876
0·26377	−0·07418	0·26767	0·71393	0·04321	−0·87738
0·22062	−0·07204	0·29658	0·76106	0·03587	−0·84494
0·18042	−0·06859	0·34148	0·80541	0·02837	−0·82224
0·14353	−0·06390	0·40522	0·84632	0·02081	−0·80861
0·11026	−0·05806	0·49105	0·88315	0·01325	−0·79910
0·08092	−0·05120	0·60201	0·91535	0·00567	−0·77853
0·05576	−0·04346	0·73856	0·94252	−0·00197	−0·71361
0·03503	−0·03501	0·88939	0·96450	−0·00956	−0·55677
0·01894	−0·02601	0·99722	0·98131	−0·01669	−0·28615
0·00767	−0·01664	0·83680	0·99297	−0·02249	0·05224
0·00138	−0·00706	−0·22489	0·99916	−0·02586	0·39390
0·00018	0·00260	−2·28898	1·0000	−0·02632	1·0000

TABLE 2(b) (Contd.)

Configuration B: Flap

ξ	η	C_p
1·33316	−0·13394	0·48606
1·33007	−0·13261	0·46862
1·32393	−0·13013	0·48011
1·31469	−0·12671	0·49580
1·30236	−0·12259	0·50996
1·28708	−0·11808	0·52043
1·26907	−0·11347	0·52623
1·24868	−0·10904	0·52686
1·22636	−0·10504	0·52209
1·20264	−0·10161	0·51182
1·17808	−0·09883	0·49604
1·15326	−0·09667	0·47483
1·12872	−0·09504	0·44837
1·10495	−0·09379	0·41696
1·08240	−0·09273	0·38108
1·06141	−0·09169	0·34141
1·04227	−0·09049	0·29886
1·02520	−0·08902	0·25460
1·01037	−0·08718	0·21011
0·99789	−0·08495	0·16732
0·98782	−0·08235	0·12944
0·98017	−0·07947	0·10470
0·97490	−0·07642	0·12388
0·97194	−0·07335	0·30980
0·97114	−0·07039	0·80403
0·97228	−0·06766	0·99609
0·97506	−0·06525	0·88061
0·97917	−0·06323	0·76871
0·98428	−0·06159	0·69482
0·99013	−0·06027	0·64346
0·99653	−0·05914	0·59892
1·00337	−0·05808	0·54813
1·01064	−0·05692	0·47988
1·01840	−0·05560	0·38539
1·02675	−0·05407	0·25970
1·03580	−0·05237	0·10305
1·04565	−0·05058	−0·07900
1·05637	−0·04885	−0·27669
1·06798	−0·04730	−0·47804
1·08046	−0·04611	−0·67091
1·09377	−0·04540	−0·84461
1·10781	−0·04531	−0·99080
1·12249	−0·04594	−1·10388
1·13766	−0·04737	−1·18089
1·15321	−0·04963	−1·22115
1·16897	−0·05276	−1·22586
1·18481	−0·05673	−1·19765
1·20056	−0·06152	−1·14016
1·21610	−0·06704	−1·05764
1·23126	−0·07322	−0·95469
1·24592	−0·07992	−0·83600
1·25994	−0·08700	−0·70610
1·27319	−0·09429	−0·56925
1·28553	−0·10161	−0·42927
1·29683	−0·10873	−0·28945
1·30696	−0·11544	−0·15242
1·31575	−0·12149	−0·02002
1·32303	−0·12663	0·10702
1·32861	−0·13061	0·23002
1·33223	−0·13318	0·35684
1·33352	−0·13408	1·0000

TABLE 3

	Main aerofoil				Flap				Total
	C_N	C_A	C_L^*	Γ	C_N	C_A	C_L^*	Γ	C_L^{**}
Exact $\bar{\eta} = 10, \alpha = 0$	1·6915	−0·08979	1·6915	0·8400	0·3366	0·08965	0·3366	0·1745	2·0290
AMOS	1·6710	−0·0891	1·6710	0·8322	0·3148	0·0831	0·3148	0·1723	2·0092
Exact $\bar{\eta} = 10, \alpha = 10$	3·0849	−0·7120	3·1617	1·5521	0·4043	0·0967	0·3814	0·2203	3·5448
AMOS	3·0515	−0·7047	3·1275	1·5440	0·3812	0·0893	0·3583	0·2189	3·5259
Exact $\bar{\eta} = 20, \alpha = 0$	2·3119	−0·2125	2·3119	1·1233	0·5936	0·2124	0·5936	0·3301	2·9068
AMOS	2·2859	−0·2093	2·2859	1·1143	0·5649	0·1966	0·5649	0·3274	2·8835
Exact $\bar{\eta} = 30, \alpha = 0$	2·9065	−0·3839	2·9065	1·3909	0·8302	0·3838	0·8302	0·4784	3·7386
AMOS	2·8700	−0·3752	2·8700	1·3777	0·7984	0·3559	0·7984	0·4737	3·7029
Exact $\bar{\eta} = 30, \alpha = 10$	4·2207	−1·2625	4·3758	2·0687	0·8392	0·3703	0·7622	0·5015	5·1404
AMOS	4·1751	−1·2425	4·3274	2·0558	0·8080	0·3423	0·7363	0·4975	5·1065
Exact $\bar{\eta} = 40°, \alpha = 0$	3·4442	−0·5951	3·4442	1·6332	1·0481	0·5948	1·0481	0·6142	4·4948
AMOS	3·4006	−0·5791	3·4006	1·6169	1·0260	0·5629	1·0260	0·6688	4·4515

* Based on integration of pressures.
** Based on overall circulation round the two aerofoils.

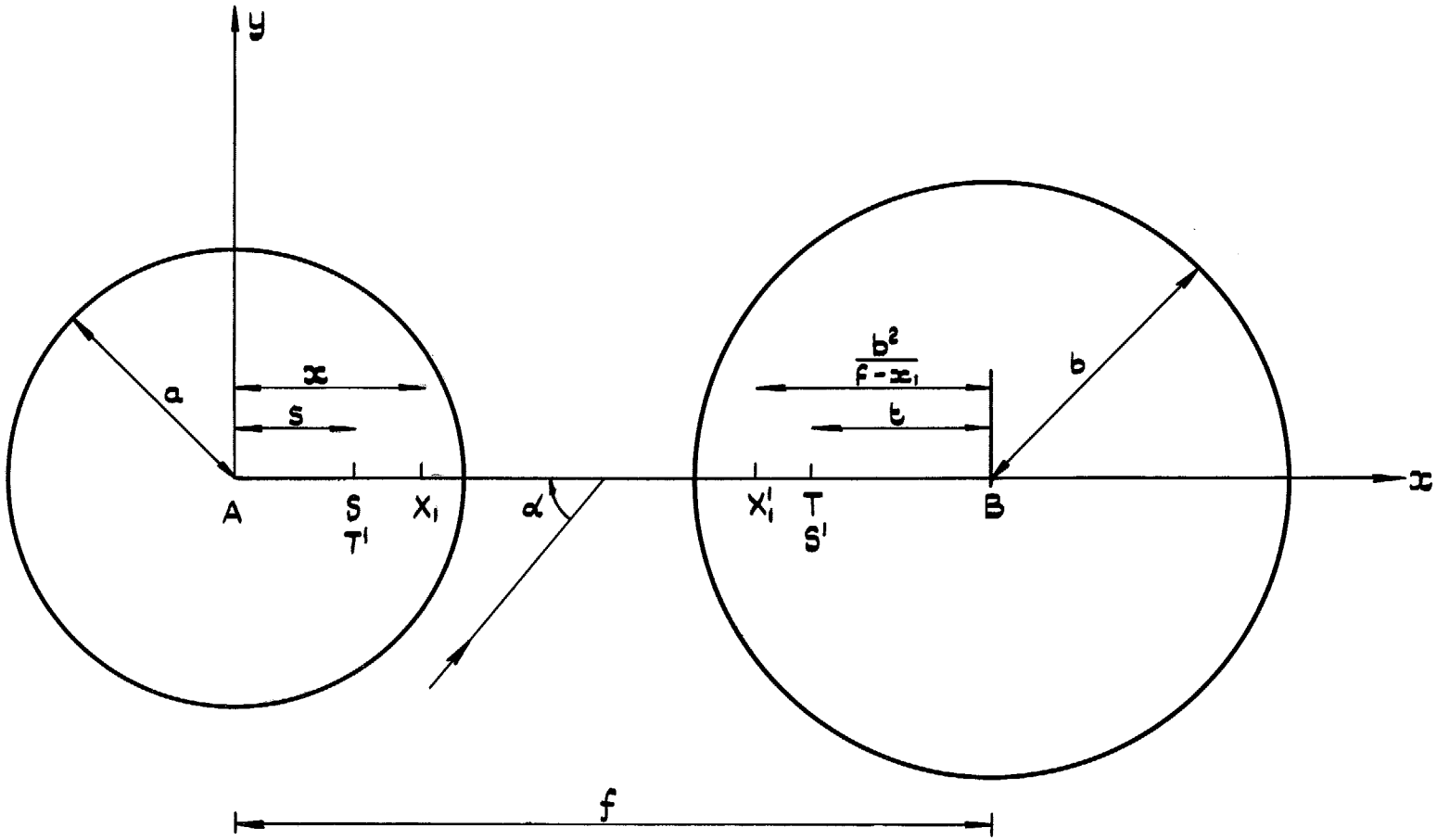

FIG. 1. Geometry of two circles.

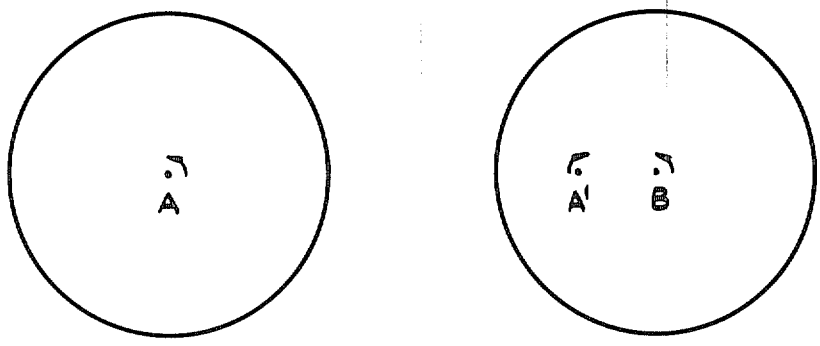

a First reflection

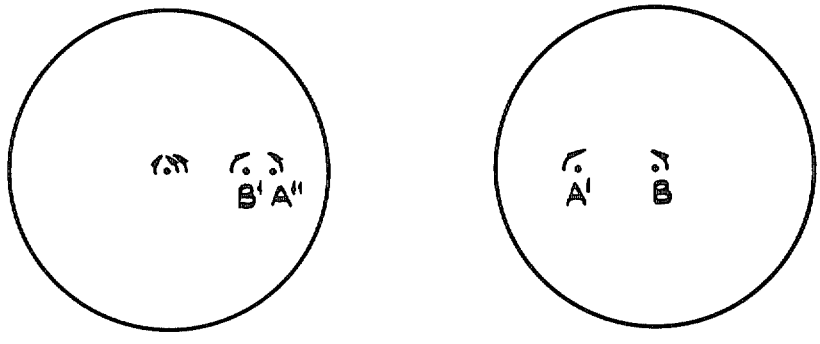

b Second reflection

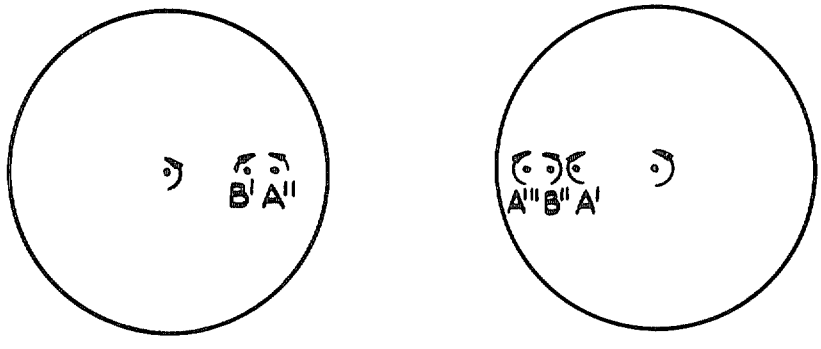

c Third reflection

FIG. 2a–c. Vortex image system.

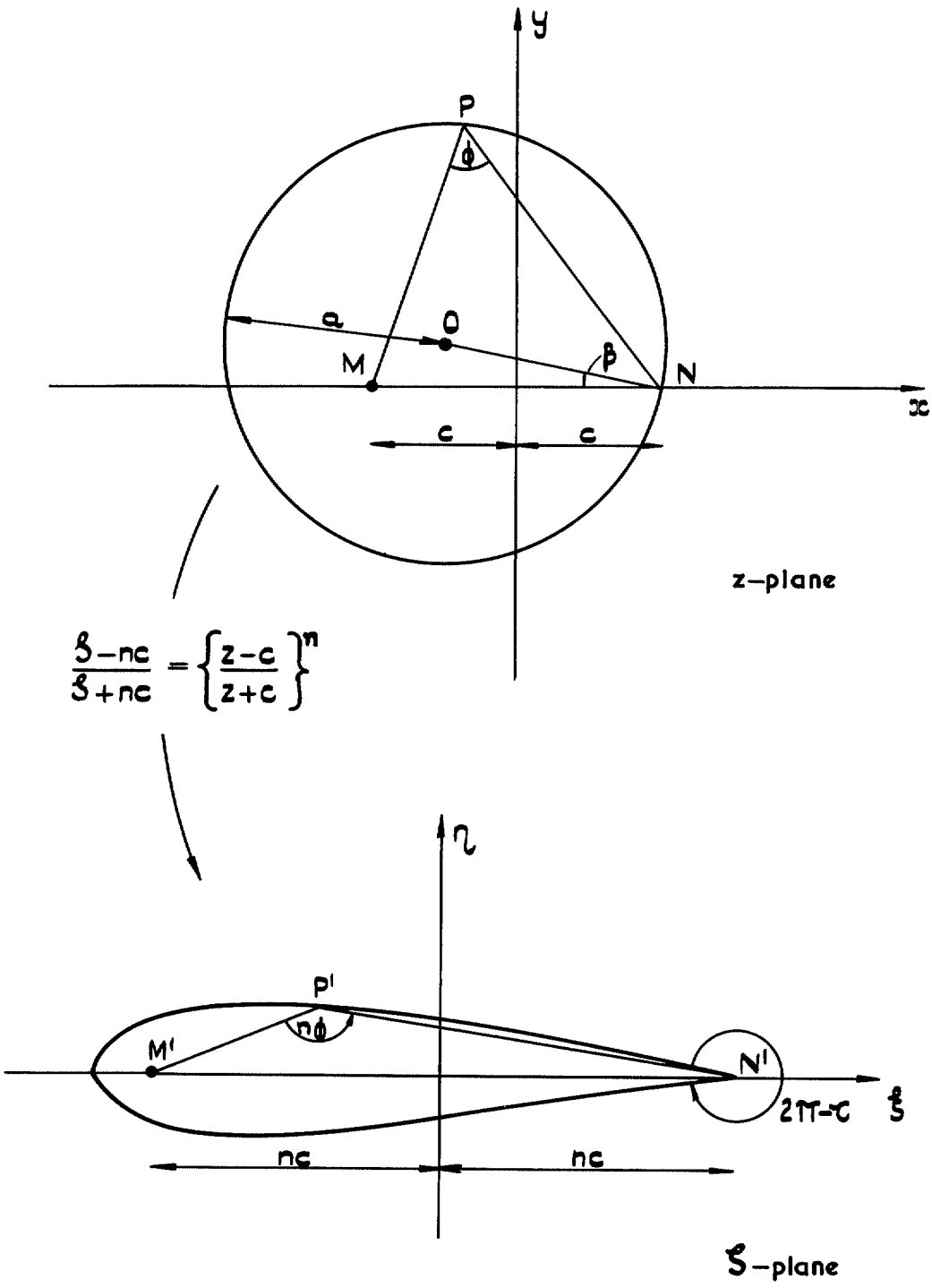

FIG. 3. Karman–Trefftz transformation.

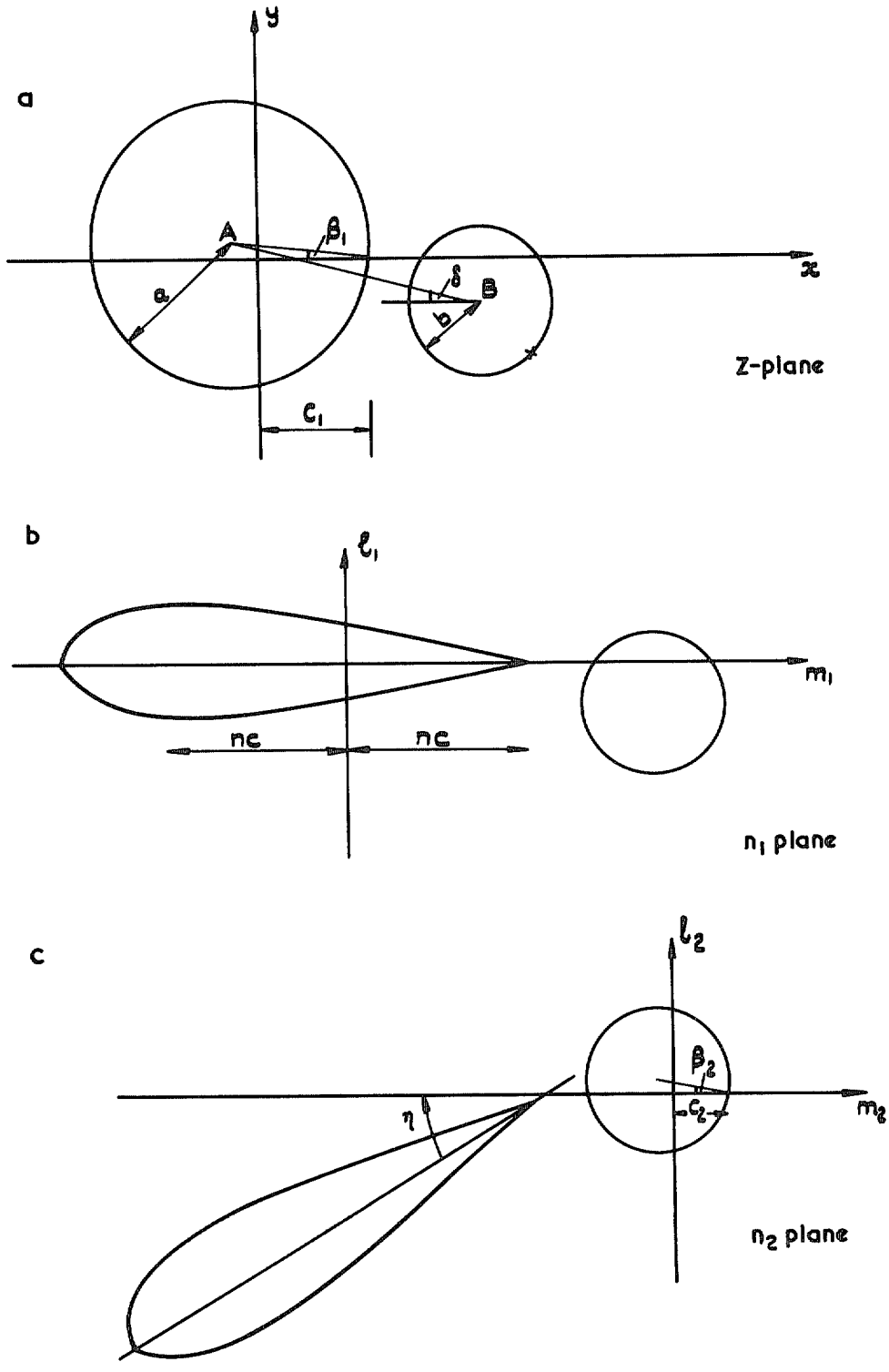

FIG. 4a–c. Karman–Trefftz transformations.

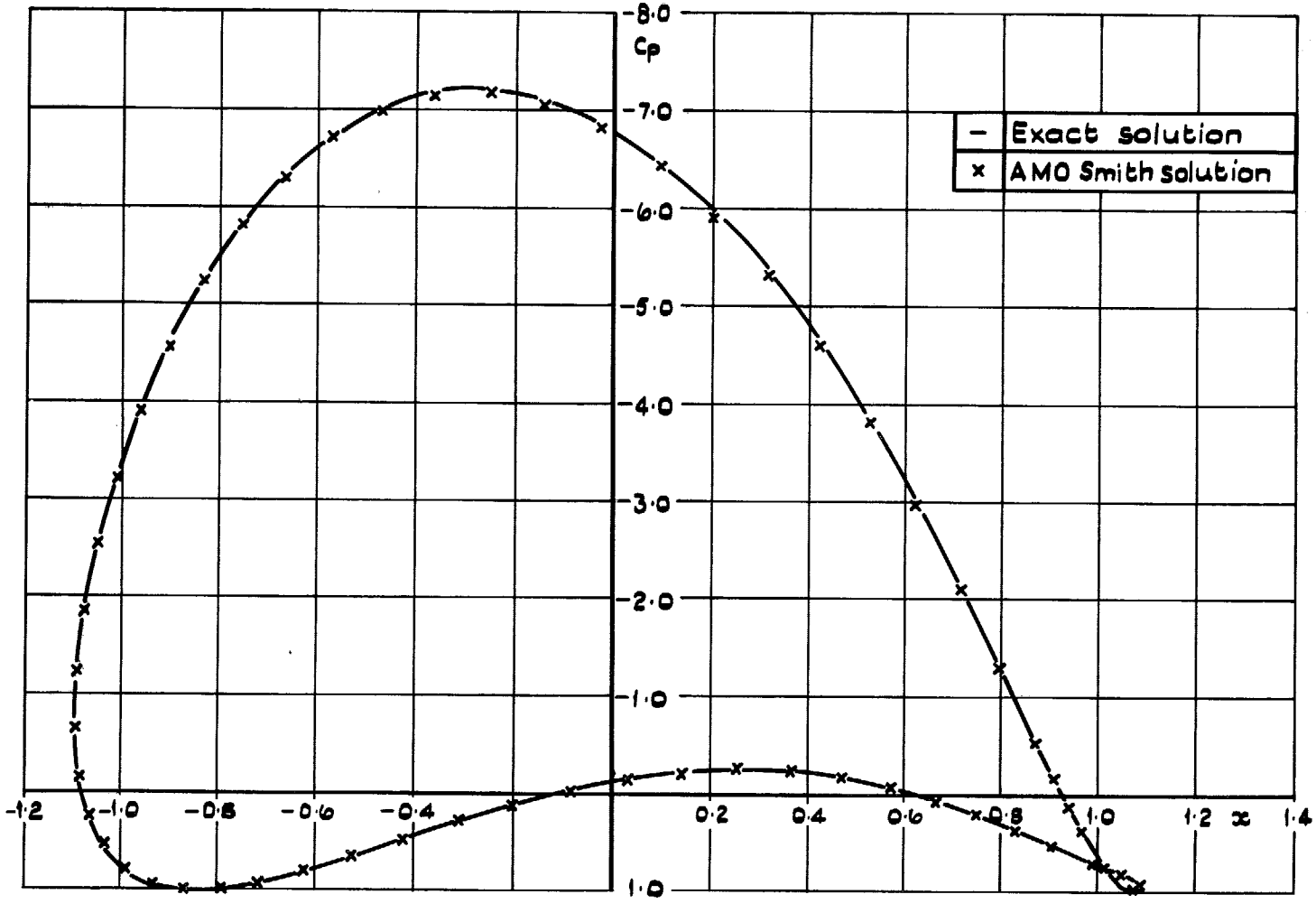

FIG. 5. Pressure distribution for first circle.

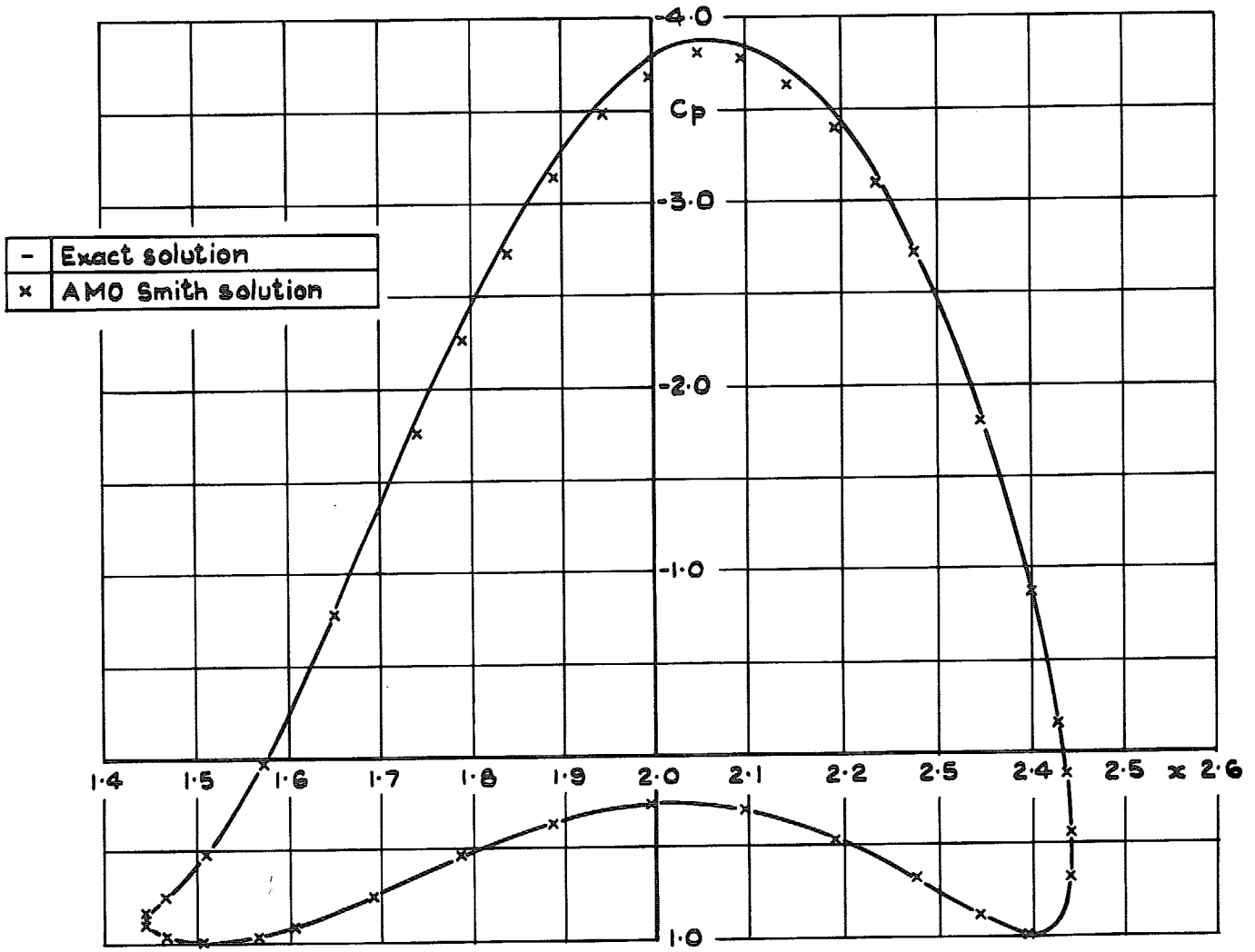

FIG. 6. Pressure distribution for second circle.

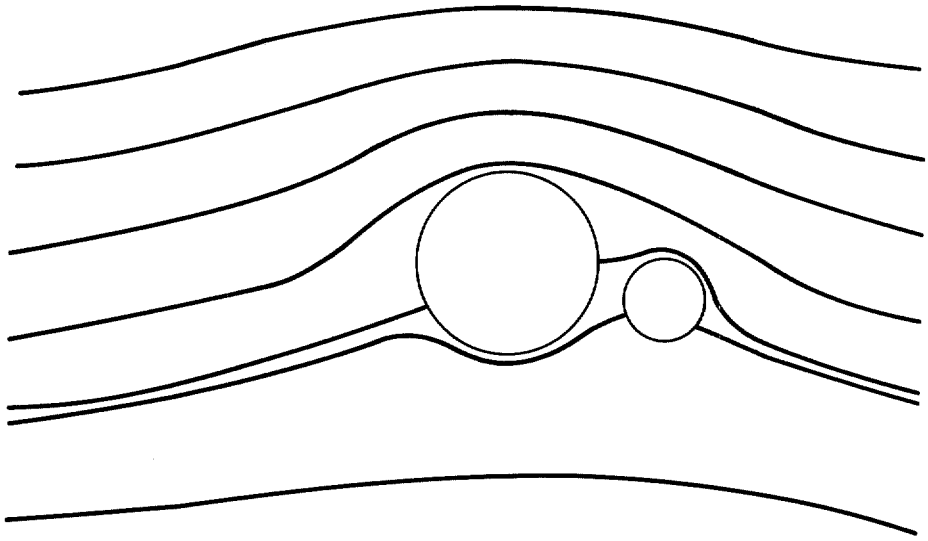

FIG. 7. Streamlines around two lifting circles.

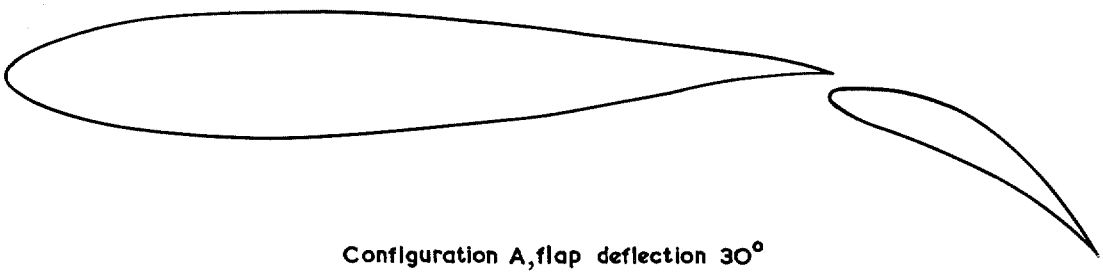

Configuration A, flap deflection 30°

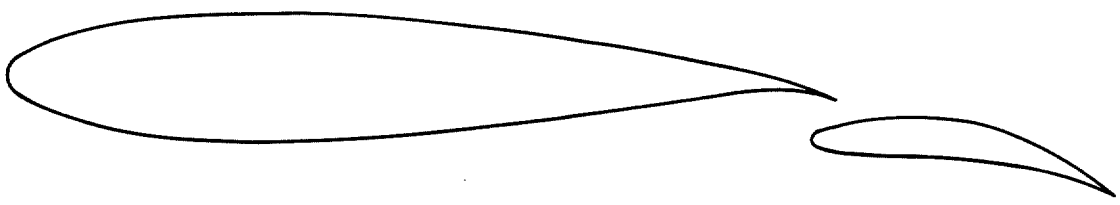

Configuration B, flap deflection 10°

FIG. 8. Configuration A and B.

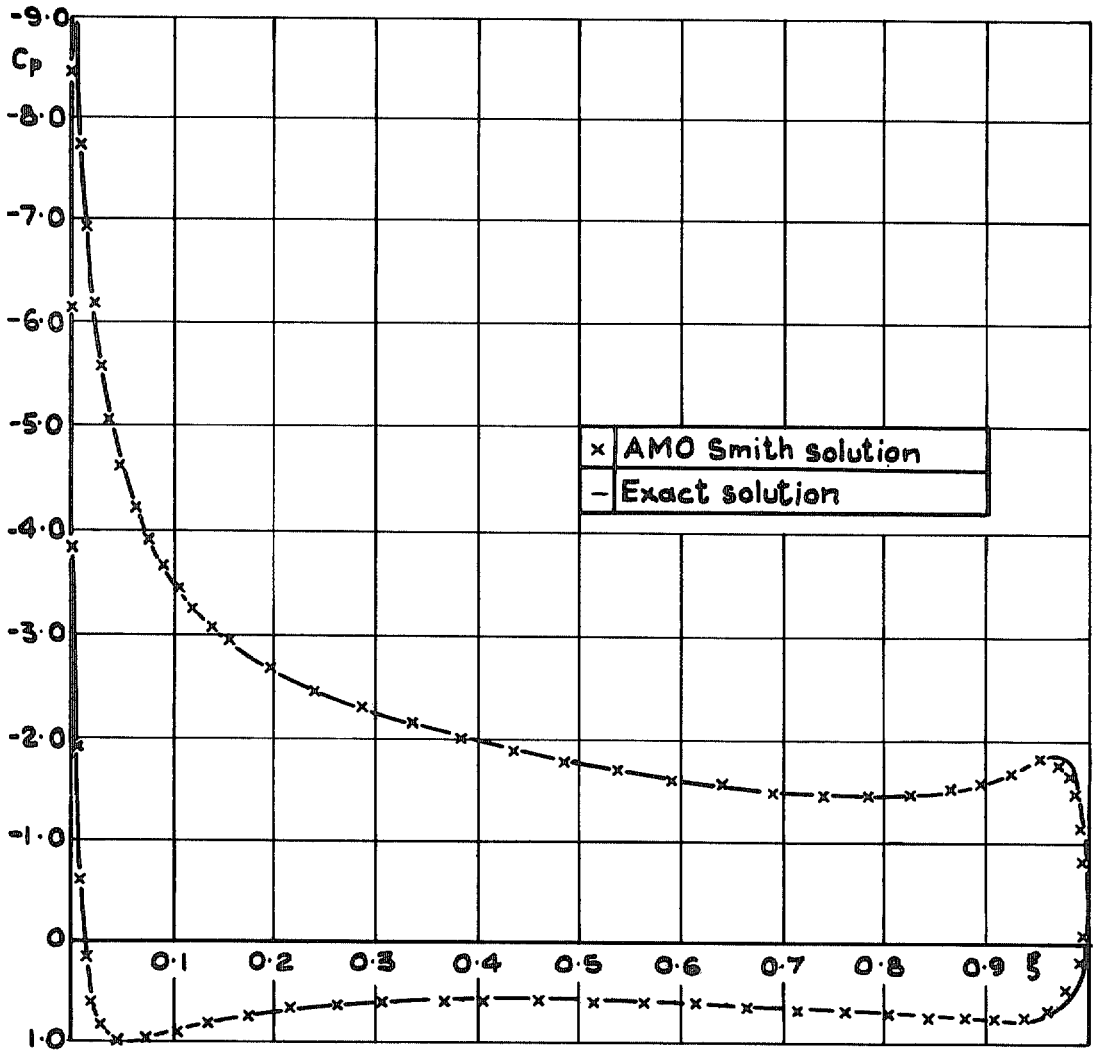

FIG. 9. Pressure distribution for main aerofoil of configuration A. Flap deflection 30°. Incidence 0°.

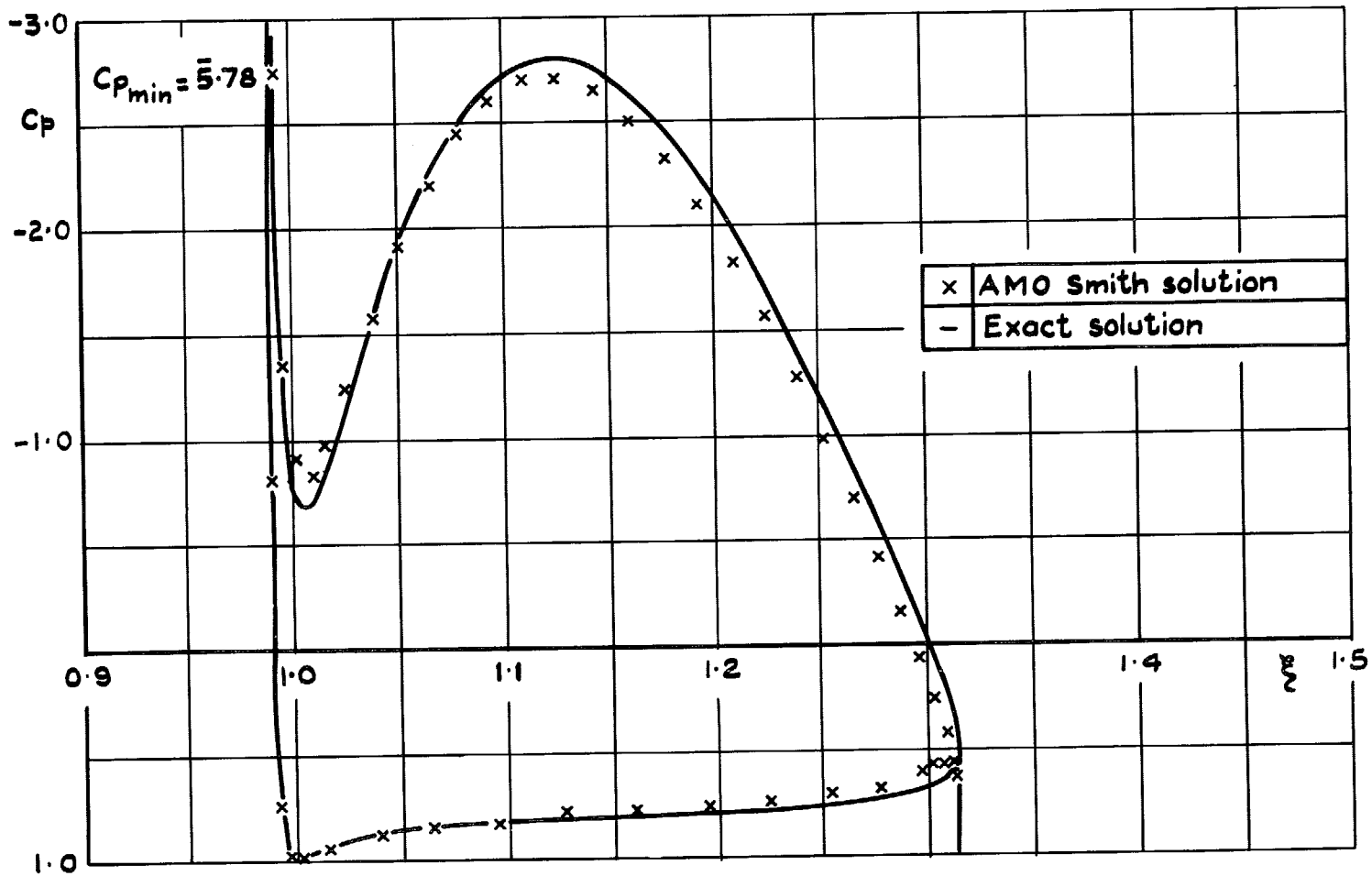

FIG. 10. Pressure distribution for flap of configuration A. Flap deflection 30°. Incidence 0°.

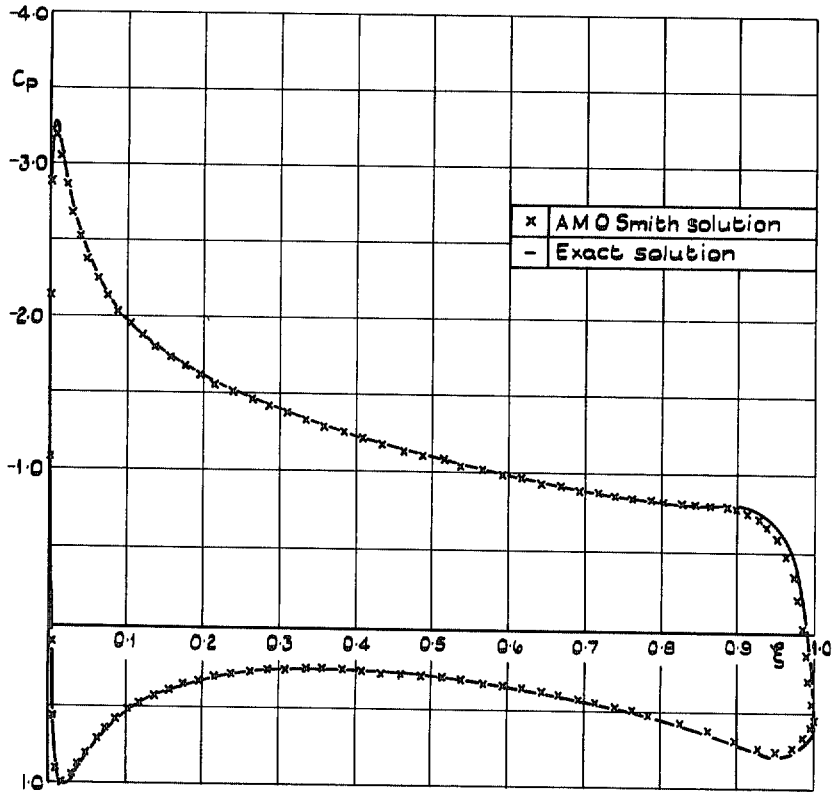

FIG. 11. Pressure distribution for main aerofoil of configuration B. Flap deflection 10°. Incidence 0°

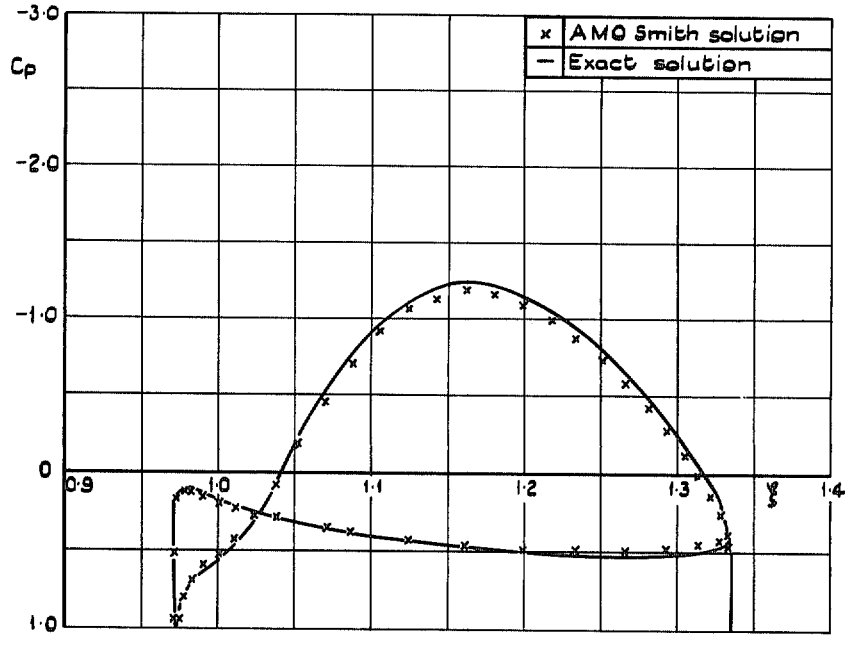

FIG. 12. Pressure distribution for flap of configuration B. Flap deflection 10°. Incidence 0°.

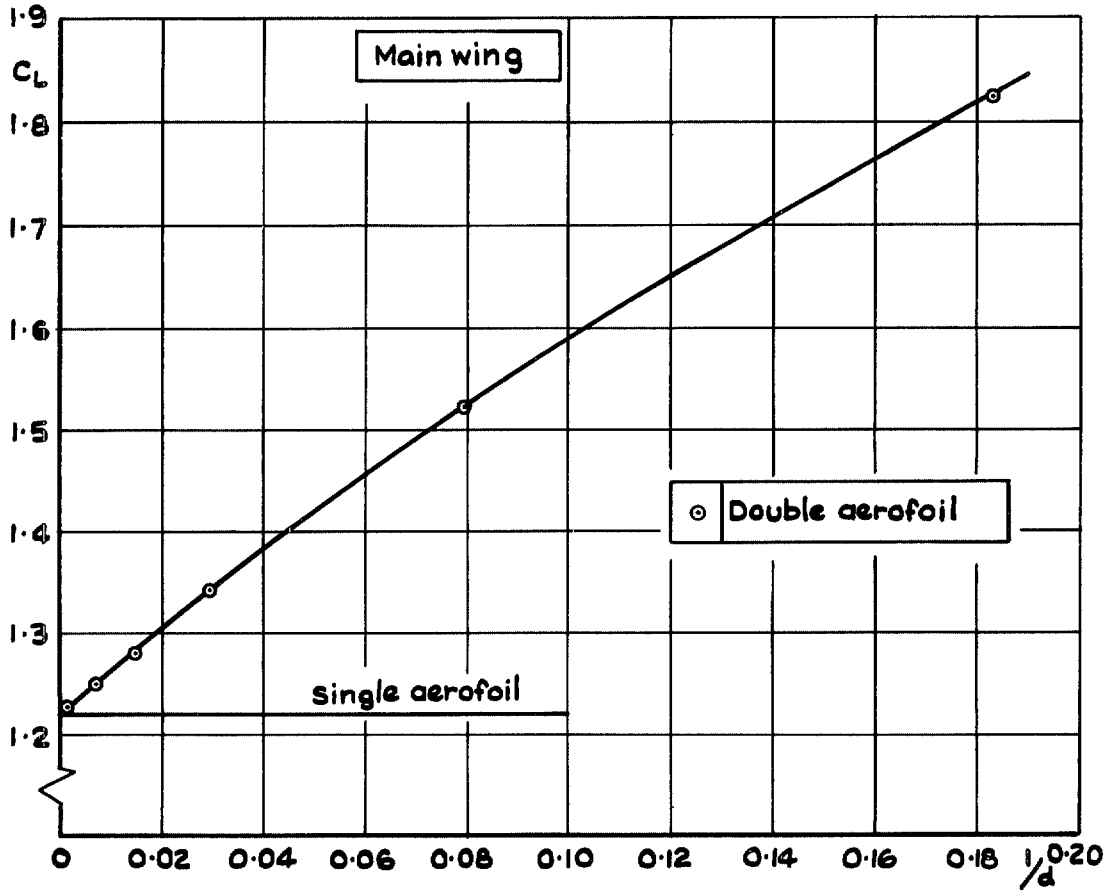

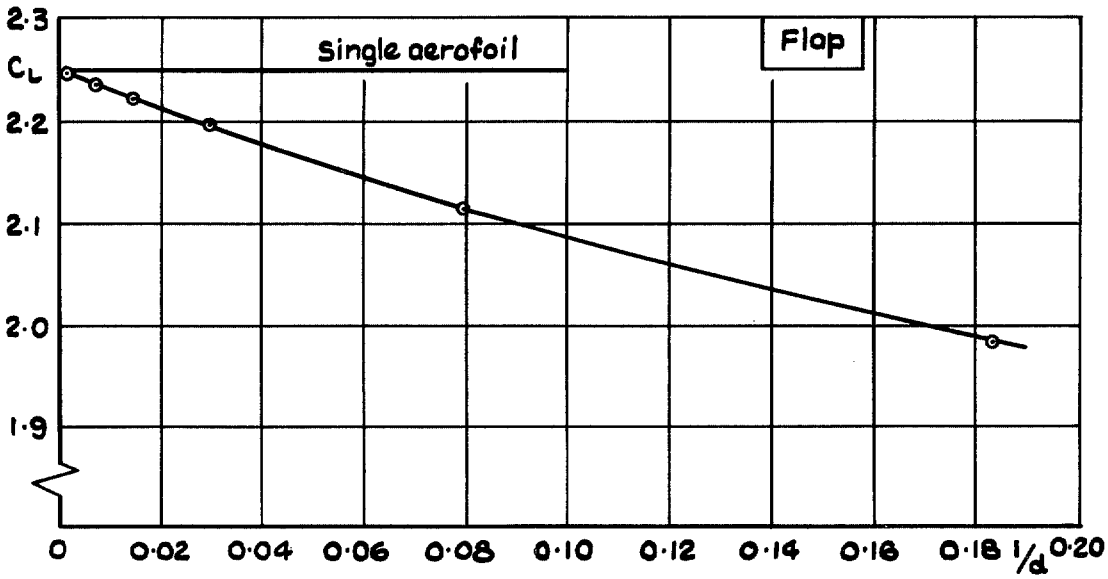

FIG. 13. Lift of aerofoils at large separation.

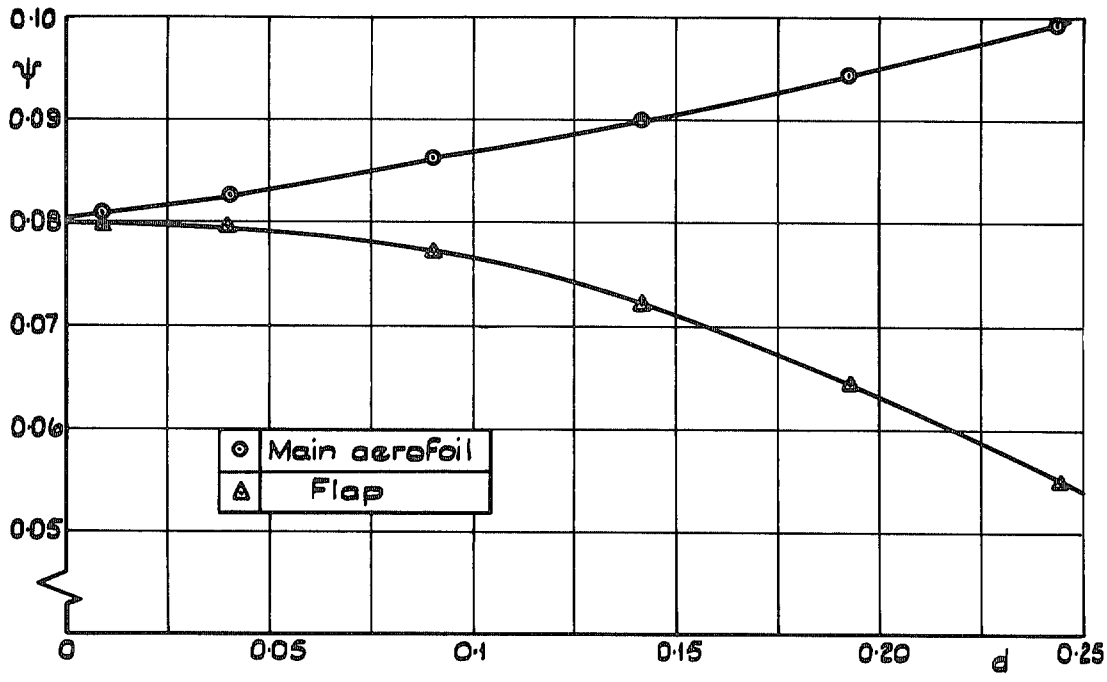

a. Stream function on aerofoils.

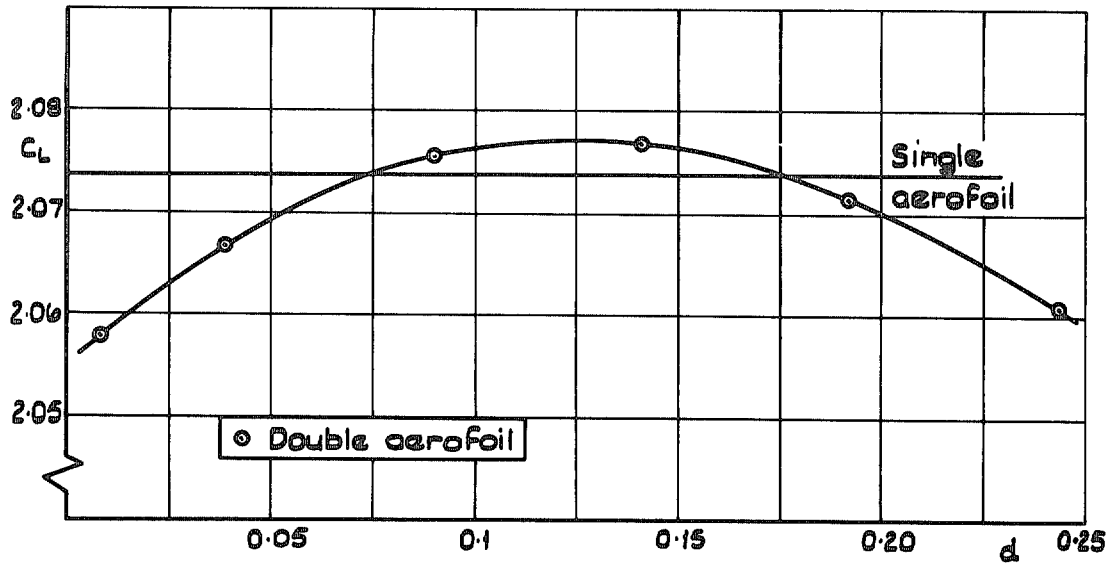

b. Total lift on aerofoils.

FIG. 14a and b. Aerofoils at small separation.

Printed in England for Her Majesty's Stationery Office by J. W. Arrowsmith Ltd., Bristol
Dd. 503426 K5 1/73

HER MAJESTY'S STATIONERY OFFICE

Government Bookshops

49 High Holborn, London WC1V 6HB
13a Castle Street, Edinburgh EH2 3AR
109 St Mary Street, Cardiff CF1 1JW
Brazennose Street, Manchester M60 8AS
50 Fairfax Street, Bristol BS1 3DE
258 Broad Street, Birmingham B1 2HE
80 Chichester Street, Belfast BT1 4JY

Government publications are also available through booksellers

SBN 11 470517 8